Journal of Alloys and Compounds 874 (2021) 159870

Contents lists available at ScienceDirect

Journal of Alloys and Compounds

journal homepage: www.elsevier.com/locate/jalcom

Unraveling the multi-featured magnetic behavior of $Nd_{0.75}Sr_{0.25}CoO_3$ perovskite nanocrystals annealed at different temperatures

Hajer Chouaibi[a], Beatriz Rivas-Murias[b,c,*], Mourad Smari[a], Jalel Massoudi[a], Essebti Dhahri[a], Verónica Salgueiriño[b,c,*]

[a] Laboratoire de Physique Appliquée, Faculté des Sciences, Université de Sfax, B.P. 1171, Sfax 3000, Tunisia
[b] Departamento de Física Aplicada, Universidade de Vigo, Vigo 36210, Spain
[c] CINBIO, Universidade de Vigo, Vigo 36310, Spain

ARTICLE INFO

Article history:
Received 4 January 2021
Received in revised form 14 March 2021
Accepted 4 April 2021
Available online 9 April 2021

Keywords:
Perovskite nanocrystals
Cobaltites
Annealing
Magnetic Measurements
Raman Spectroscopy

ABSTRACT

Perovskite nanocrystals are gaining increased attention because of their magnetic, transport and catalytic properties, and particularly there is a renewable interest of cobalt perovskites for catalysis. Accordingly, the correct interpretation of their properties stemming from a particular configuration of the cations within this crystalline structure is compulsory. Herein, we report the synthesis of $Nd_{0.75}Sr_{0.25}CoO_3$ nanocrystals using the citrate sol-gel method and annealed at different final temperatures (600 °C, 700 °C, 800 °C and 1150 °C). Their characterization was carried out combining transmission electron microscopy, X-ray diffraction, Raman spectroscopy and vibrating sample magnetometry, demonstrating their complementarity to get the whole picture of the multi-featured perovskite-based nanocrystal behavior.

© 2021 Elsevier B.V. All rights reserved.

1. Introduction

Perovskite nanocrystals with magnetic, transport and catalytic properties have been reported to lead to a unique set of physical phenomena, which can be considered independently or interrelated for different applications [1–6]. For example, concerning the field of catalysis, the current and worrying situation of our planet in terms of global warming and the depletion of the fossil fuels has increased a renewable interest in electrocatalysts, and in particular the study of the performance of cobalt perovskite oxides [7–11].

Focusing on the family of perovskite cobaltites, $Ln_{1-x}A_xCoO_3$, where Ln corresponds to lanthanides and A to alkaline-earth metals, they show significant features stemming from the crystalline structure and the configuration of the different cations in it. We can refer the cobalt ion spin-state, which is not present in the manganite counterpart, and becomes as an additional degree of freedom for the colossal magnetoresistance effect [12–16]. In fact, in the cobaltites, the comparable size between the Hund's rule exchange and the crystal field splitting energies induces an easy coexistence of low, intermediate and high spin state for Co^{3+} and the presence of Co^{4+} in these systems, offering a new degree of freedom and therefore a playground of possibilities [17,18]. Another important issue, characteristic of cobalt perovskites but also of other complex oxides, relates to the magnetoelectronic phase separation, if the system is doped with a divalent cation at the A site [19–21]. As a consequence, there is heterogeneity in the magnetic and electronic properties even without a chemical segregation [13,22–24]. Furthermore, studies about the $Nd_{1-x}Sr_xCoO_3$ family, while being less studied than its lanthanum-based counterpart, have focused on the region where ferrimagnetism dominates [25], given the fact that, the presence of the smaller neodymium cation leads to a decrease in bandwidth in comparison to the lanthanum family, with consequences in the competing magnetic interactions and the metal-insulator phenomena [26]. In this context, herein we report about the structural and magnetic characterization of $Nd_{0.75}Sr_{0.25}CoO_3$ nanocrystals, synthesized by the citrate sol-gel method and annealed at different final temperatures (600 °C, 700 °C, 800 °C and 1150 °C). The sol-gel method employed to synthesize these samples favors the formation of pure phases at lower temperatures, in comparison to the typical solid-state reaction, and offers control over the porosity and the particle size. The magnetic scenario of these perovskite-based nanocrystals can be assessed and understood using a combination of different techniques (transmission electron microscopy, X-ray diffraction, Raman spectroscopy and vibrating sample magnetometry),

* Corresponding authors at: Departamento de Física Aplicada, Universidade de Vigo, Vigo 36210, Spain.
E-mail addresses: brivas@uvigo.es (B. Rivas-Murias), vsalgue@uvigo.es (V. Salgueiriño).

https://doi.org/10.1016/j.jallcom.2021.159870
0925-8388/© 2021 Elsevier B.V. All rights reserved.

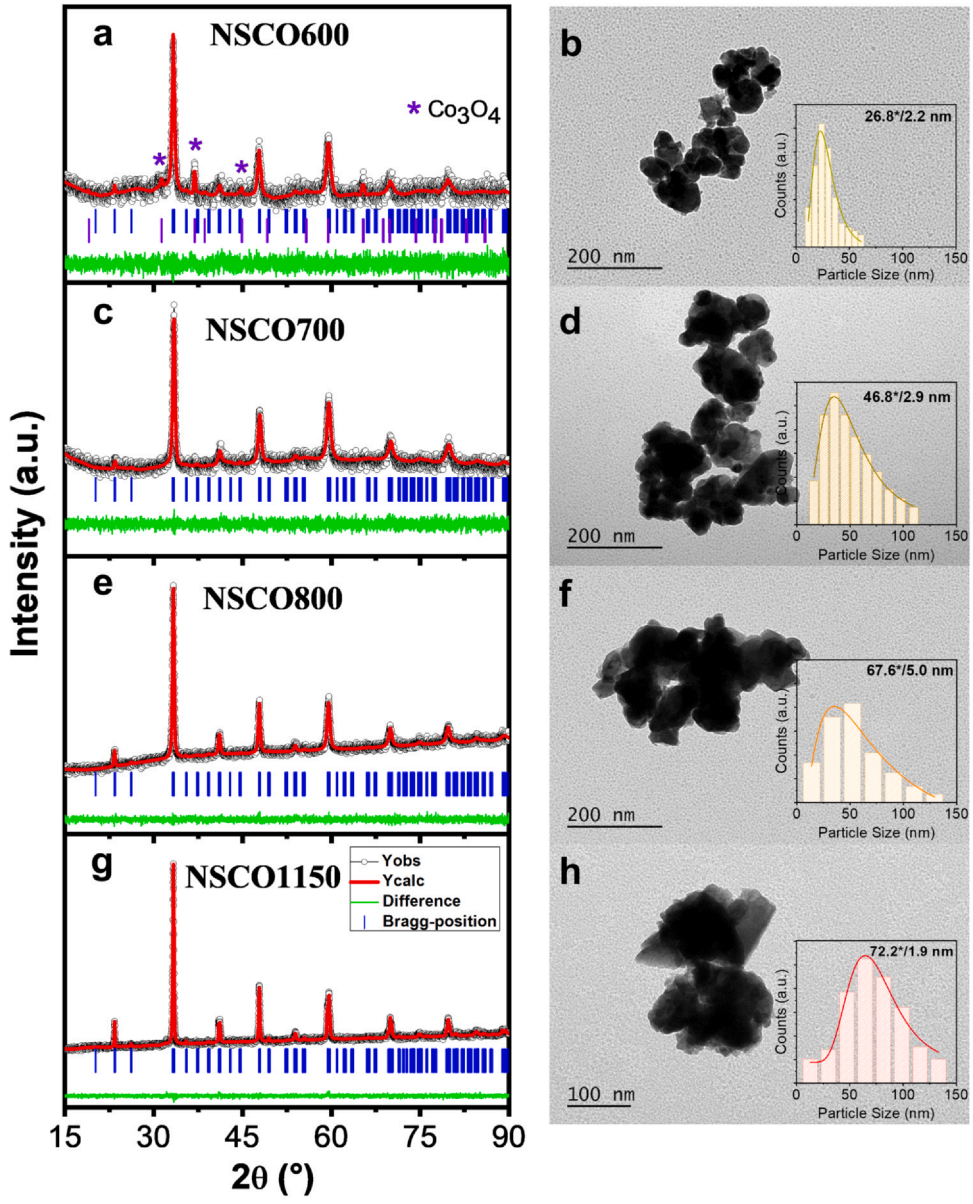

Fig. 1. XRD patterns with the Rietveld refinement and representative TEM images of the $Nd_{0.75}Sr_{0.25}CoO_3$ nanocrystals from the NSCO600 (a and b), NSCO700 (c and d), NSCO800 (e and f) and NSCO1150 (g and h) samples. The black circles in the XRD patterns represent the experimental data, the continuous red line is the fitted curve, the vertical blue/violet lines are the Bragg positions, and the difference between experimental and fitted patterns is shown as a solid green line at the bottom. Inset: The size distribution histograms are fitted to log-normal curves.

demonstrating their complementarity to understand the different effects, stemming from stoichiometry and crystalline structure, characteristic of these nanocrystals. Accordingly, while checking the effect the annealing temperature can exert in the structural and magnetic properties of the $Nd_{0.75}Sr_{0.25}CoO_3$ material, we prove the Raman spectroscopy as a unique technique for the effective identification of secondary phases in an easy and non-destructive way, attaining a detailed and complete characterization of the systems.

2. Experimental section

2.1. Synthesis

$Nd_{0.75}Sr_{0.25}CoO_3$ (NSCO) nanocrystals were prepared by a two-step synthetic method considering the citrate sol-gel route using Nd $(NO_3)_3{\cdot}H_2O$, $Sr(NO_3)_2$ and $Co(NO_3)_2{\cdot}6H_2O$ with 99.9% purity (purchased from Sigma Aldrich, as precursors) and an annealing final process at different temperatures (600 °C, 700 °C, 800 °C and 1150 °C). The initial solution was prepared by mixing stoichiometric amounts of nitrates in distilled water. Then, citric acid ($C_6H_8O_7$, as chelating agent, in a metal cation (Nd+Sr+Co) to citric acid molar ratio equal to 1:2) and 1 mL of ethylene glycol ($C_2H_6O_2$) were added to the previous solution. This solution was stirred and heated up to 80 °C and kept at this temperature for 3 h until obtaining a viscous gel. After that, this gel was heated on a hot plate up to 180 °C to obtain a powder, which was then thoroughly ground and firstly calcined in air at 400 °C during 12 h and finally at 500 °C for 24 h. This step is performed in order to ensure the complete removal of the organic compounds from the powders. Finally, the samples were left to cool down (3 °C per minute) and the different black powders

were pressed into pellets (5 tons per cm^2) and annealed at 600 °C (the sample is labeled as NSCO600), 700 °C (NSCO700) or 800 °C (NSCO800) for 12 h, and at 1150 °C (NSCO1150) for 24 h.

2.2. Characterization

The pellet X-ray diffraction (XRD) patterns were collected using a X′Pert PRO MPD Diffractometer (Cu K_α radiation, Bragg-Brentano θ-2θ geometry) in the 2θ angular range of 15–90°. The XRD patterns were analyzed by Rietveld refinement using the FULLPROF software. Transmission electron microscopy (TEM) images were performed on a JEOL JEM1010 instrument operating at an acceleration voltage of 100 kV. Samples for TEM analysis were prepared by dropping a diluted suspension of the nanocrystals from the pellets onto an ultrathin carbon coated copper grid. Raman spectra were collected with a Renishaw in Via Reflex confocal Raman Microscope. Experiments were conducted at room temperature using a 785 nm laser excitation wavelength. The laser beam was focused on the sample by a 20x or 50x objective, with a numerical aperture (NA) value of 0.40 or 0.75, respectively. The laser power on the sample surface used was varied from 0.1% to 50% (from ~0.6 mW to ~31 mW), such that lower values were used to avoid any possible modifications on the surface sample and higher values were used to study the sample evolution. Note here that for 10% and 50% of laser power the spectra were collected at 0.1% of laser power (~0.6 mW) after applying these higher powers, due to the detector saturation. Magnetic measurements were performed using the Vibrating Sample Magnetometer (VSM) option in a Physical Property Measurement System (PPMS) from Quantum Design. The temperature-dependent magnetization using zero-field-cooled (ZFC) and field-cooled (FC) conditions was performed at 50 or 500 mT in the 10–300 K range. Hysteresis loops under ZFC conditions were measured at 10, 50 and 125 K, applying magnetic fields up to 7 T.

3. Results and discussion

The $Nd_{0.75}Sr_{0.25}CoO_3$ nanocrystals forming part of the four samples in consideration, were synthesized by the citrate sol-gel method and additionally annealed at the different temperatures (600 °C, 700 °C, 800 °C and 1150 °C), from now on referred to as NSCO600, NSCO700, NSCO800 and NSCO1150 samples, respectively. The XRD patterns of these samples collected at room temperature are shown in Fig. 1 (left column). According to these diffraction patterns, all the samples crystallize in an orthorhombic structure (*Pbnm* space group, no. 62), where the lattice parameters are ~$\sqrt{2}a_p \times \sqrt{2}a_p \times 2a_p$ (a_p~0.374 nm refers to the lattice parameter for the ideal cubic perovskite structure). These XRD patterns were analyzed by the Rietveld refinement method [27] and the lattice parameters and atomic positions obtained are displayed in Table 1. As increasing the temperature at which the samples were annealed, the lattice parameters are in better agreement with those reported for similar strontium doped neodymium cobaltites [19]. The average crystallite (D_{sc}) size can be calculated from the line broadening of the peaks using the classical Scherrer formula [28], $D_{SC} = K\lambda/\beta\cos\theta$, where K is the shape factor (equal to 0.9 for spherical particles), λ is the radiation wavelength, θ the diffraction Bragg angle and β is the full width at half the maximum (FWHM) of the peak (in radians and after subtracting the FWHM value coming from the instrumental factors). A rough analysis of the line broadening of the most intense peak (corresponding to (112) planes, see the indexed diffracted peaks in Fig. 1g), using equation 1 and Lorentzian profiles, offers average crystallite sizes of ~17, ~19, ~26 and ~36 nm for the NSCO600, NSCO700, NSCO800 and NSCO1150 samples, respectively, revealing therefore that the average crystallite size increases the larger the annealing temperature, because of a more effective sintering process of the initial nuclei formed in the synthetic sol-gel stage.

Taking the limit of the detection of the technique into account, while the NSCO800 and NSCO1150 samples can be described in terms of a perovskite single phase, the NSCO600 sample shows the presence of different extra peaks, with the one located at 37° corresponding to the most intense peak of the Co_3O_4 phase (~12.88 wt %), with a spinel crystalline structure [31]. Likely, a small amount (though below the limit of detection of the technique) of this secondary Co_3O_4 phase is also present in the NSCO700 sample, in view of the large difference registered between the fitted and diffracted pattern when performing the Rietveld refinement.

The morphology and the average size of the $Nd_{0.75}Sr_{0.25}CoO_3$ nanocrystals in the four different samples were studied by TEM (Fig. 1), reflecting the irregular shape and an increase in the average size of the nanocrystals stemming from increasing the annealing temperature. A larger temperature of annealing during this second synthetic step promotes an increase of the average sizes of both, the crystalline domain and of the nanocrystals themselves, due to the coalescence of the initial crystallites formed during the nucleation step in the sol-gel process [32]. The size distribution analysis of the four samples are shown in Fig. 1 (insets in the right column) and fitted to log-normal functions [33], offering average diameters of 26.8*/2.2, 46.8*/2.9, 67.6*/5.0 and 72.2*/1.9 nm (95.50% of confidence interval) for the NSCO600, NSCO700, NSCO800 and NSCO1150 samples, respectively. The fact of having larger sizes of nanocrystals as reflected in the TEM but smaller crystallite domains from the XRD analysis, just proves that the nanocrystals are polycrystalline in the four samples.

Raman spectroscopy has been widely used as an effective tool to investigate cation disorder, lattice dynamics and structure transitions in perovskites due of its sensitivity and high spatial resolution to explore the atomic vibrations related [34]. Furthermore, this technique has been demonstrated to be very useful to further corroborate a single-phase or the presence of secondary phases in the

Table 1
Summary of the Rietveld refined parameters from the XRD data of the nanocrystals from the NSCO600, NSCO700, NSCO800 and NSCO1150 samples, considering the *Pbnm* space group. While Nd, Sr and O(1) atoms occupy the 4c (x, y, 1/4), Co and O(2) atoms are in the 4b (0, 1/2, 0) and 8d (x, y, z) Wyckoff positions, respectively [29,30].

Samples		NSCO600	NSCO700	NSCO800	NSCO1150
a (nm)		0.53894(17)	0.5398(2)	0.53977(12)	0.53994(3)
b (nm)		0.53611(3)	0.53658(20)	0.53667(9)	0.53611(3)
c (nm)		0.7609(2)	0.7583(3)	0.75980(12)	0.75972(4)
V (nm^3)		0.21985(9)	0.21963(15)	0.22009(7)	0.21992(2)
Length (Å)	Co-O(1)	1.907(8)	1.926(17)	1.939(12)	1.924(4)
	Co-O(2)	1.80(5)	1.92(7)	1.89(4)	1.95(3)
	Co-O(2)	2.30(6)	2.12(7)	1.98(4)	1.91(3)
Angle (°)	Co-O(1)-Co	171.6(3)	159.6(7)	156.8(5)	161.4(18)
	Co-O(2)-Co	136(2)	140(3)	158.3(18)	159.8(11)
R_p (%)		6.72	2.33	5.19	3.33
R_{wp} (%)		8.13	2.40	6.33	4.99
χ^2		1.14	1.12	1.14	1.18

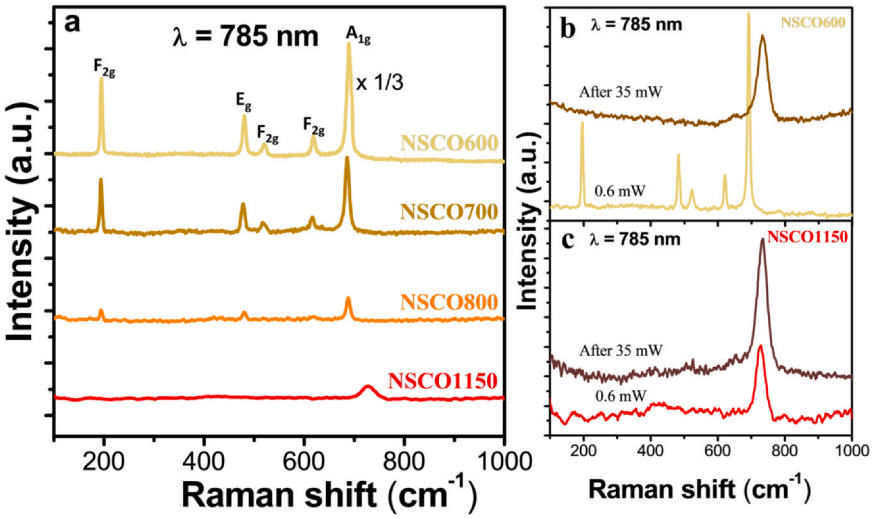

Fig. 2. Stokes-shifted Raman spectra (obtained using a 785 nm excitation wavelength and 0.6 mW of laser power) of nanocrystals from the NSCO600, NSCO700, NSCO800 and NSCO1150 samples (a) and Raman spectra applying a 0.6 mW laser power before and after applying a 35 mW laser power to the nanocrystals from the NSCO600 (b) and NSCO1150 (c) samples.

samples to be analyzed. The *Pbnm* space group of the perovskite crystalline structure in which the studied samples crystallize presents, according to group theory, 24 Raman active modes: $7A_g + 7B_{1g} + 5B_{2g} + 5B_{3g}$, which corresponds to $7A_g + 5B_{1g} + 7B_{2g} + 5B_{3g}$ in the *Pnma* coordinate system [35], but all are usually observed at low temperatures and using different polarizations.

The Raman spectra (shown in Fig. 2a) were performed at room temperature in the region from 100 cm^{-1} to 1000 cm^{-1} and using a 785 nm laser excitation with a 0.6 mW laser power. A main broad bands is registered in the room-temperature spectrum of the NCSO1150 sample (in red), which stem from Raman scattering of higher order, that is, from multiphonon summation processes which split on cooling [36]. Nevertheless, an additional small broad band is better appreciated in the normalized spectrum and indicated with black arrow in Fig. S1, in the Supporting Information (SI). The main feature of this NSCO1150 Raman spectrum is the presence of a relatively intense peak at 728 cm^{-1} associated to the perovskite phase. This mode corresponds to a Co–O bond-stretching (breathing mode) with B_{1g} symmetry, similarly to that observed at 610 cm^{-1} in the $LaMnO_3$ material which crystallizes in the same space group [35,37]. The peak at lower wavenumber is related to the bending vibrations of the octahedra in the perovskite structure [38]. The Raman spectra of the samples annealed at lower temperatures are completely different and show vibration peaks corresponding to the Co_3O_4 [39,40], with the Raman-active characteristic modes of the spinel structure. These are the A_{1g} and E_g plus three T_{2g} modes, being the A_{1g} the most intense (see the mode assignations in the NSCO600 sample spectrum in Fig. 2a). Therefore, the Raman analysis just confirms the presence of this cobalt oxide in the NSCO600, NSCO700 and even in the NSCO800 samples (on which this phase is not detected by XRD). The absence of the Raman modes associated to the perovskite in the spectra of the NSCO600, NSCO700 and NSCO800 samples can be explained taking the much larger intensity of the spinel vibration modes into account, which therefore screen the cobaltite modes.

Besides the advantage of distinguishing the phases in a sample, Raman spectroscopy can be useful to follow the changes that a high laser power can induce locally on the samples, in terms of crystalline structure modification, oxidation and/or evolution to other phases in a controllable way [39,41,42]. These modifications are produced due to a very local heating induced by the applied laser and the resulting process is similar to heating the material in air. With this into account, spectra from the NSCO600 and NSCO1150 samples were obtained using a 0.1% laser power (~0.6 mW), before and after exposing both samples to a laser power of 35 mW in the same spot. While the initial spectrum of the NSCO600 sample (Fig. 2b) evolves to the similar spectrum taken from NSCO1150 sample at the lowest laser power, no changes in the spectrum are induced after applying the higher power laser to the NSC1150 sample (see Fig. 2c), corroborating in this later case that the synthesized sample corresponds to a stable perovskite phase. This means that there is a reconfiguration and therefore an induced transition by which the cations and anions in the Co_3O_4 phase become part of the final perovskite phase. This also demonstrates that an extra thermal energy is necessary to obtain the same perovskite crystalline structure in the NSCO600 sample as in the NSCO1150 sample. Summarizing this part, the scenario obtained by Raman spectroscopy shows the presence of Co_3O_4 as a secondary phase in the samples synthesized below 1150 °C, coexisting together with the neodymium doped cobaltite phase shown by the XRD analysis.

Attending now to the magnetic characterization, the temperature dependence of the magnetization under ZFC (zero-field-cooled) and FC (field-cooled) conditions and applying an external field of 500 mT for the NSCO600, NSCO700, NSCO800 and NSCO1150 samples is shown in Fig. 3 (left column). The four samples exhibit an increase in the FC magnetization as the temperature decreases, showing the transition associated to the cobalt sublattice ordering ferromagnetically around ~175, 212, 165 and 113 K for NSCO600, NSCO700, NSCO800 and NSCO1150, respectively (data taken from the minimum in the derivative of the magnetization with temperature, see Fig. S2 in the SI). However, while the FC curve for the NSCO600 sample increases gradually as the temperature decreases, this FC curve reaches a maximum at low temperature and begins to decrease for the other three samples (NSCO700, NSCO800 and NSCO1150). The behavior can be associated to a ferrimagnetic ordering between the neodymium ions and the cobalt sublattice (antiparallel coupling), which reduces the net magnetization below 30–35 K for this $Nd_{0.75}Sr_{0.25}CoO_3$ magnetic phase. The coexistence of this ferri- and ferromagnetic ordering below this temperature was already reported for samples with a strontium doping between 0.20 and 0.60 [22,30]. This transition is not observed in the case of NSCO600 sample because of the more important percentage of the Co_3O_4, that is, the larger phase segregation ($Nd_xSr_yCo_zO_3$ and Co_3O_4) present. The observed maxima for the corresponding ZFC curves shift to lower temperatures and become narrower as the annealing temperature increases, in agreement with the phase transition mentioned, except for the NSCO600 sample. This NSCO600 sample

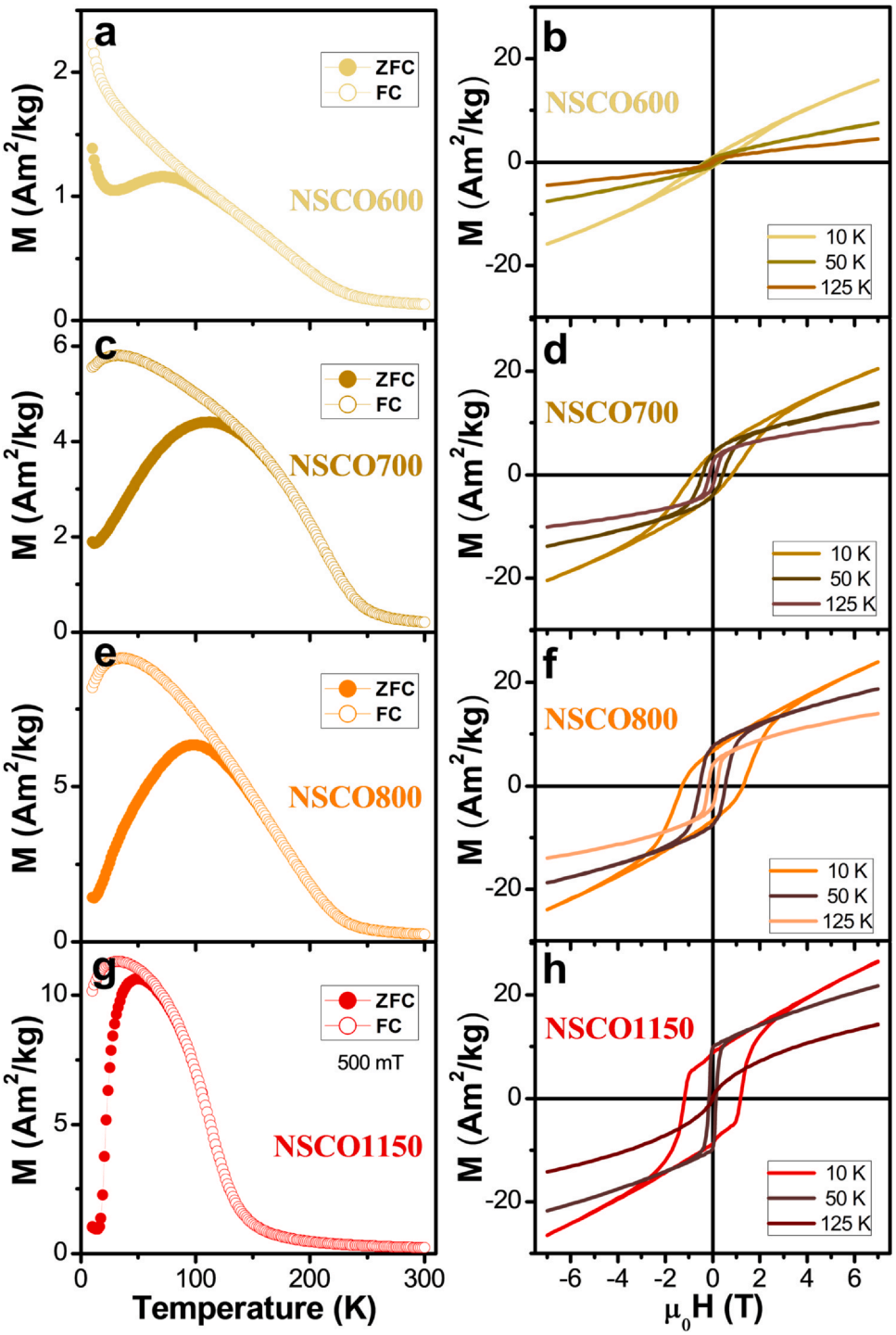

Fig. 3. ZFC-FC curves measured under an applied field of 500 mT (left column) and hysteresis loops at 10 K, 50 K and 125 K (right column) of the NSCO600 (a and b), NSCO700 (c and d), NSCO800 (e and f) and NSCO1150 (g and h) samples.

shows a maximum around 75 K, but with the magnetization curve increasing again at very low temperature, likely because of the larger phase segregation ($Nd_xSr_yCo_zO_3$ and Co_3O_4) present in this sample, as aforementioned.

The ZFC and FC curves bifurcate below a certain temperature (see Fig. 3, left column). This bifurcation reported in several doped cobaltites has been explained considering the magnetic frustration or glassy behavior [43–47], which we confirm in these samples when measuring the ZFC-FC temperature-dependent magnetization curves applying different magnetic fields [48]. Fig. S3 (in the SI) reflects this feature associated to the spin-glass behavior, with the shift of the cusp in the ZFC curve to lower temperatures and the broadening of the peak when increasing the applied field (μ_0H) from 50 to 500 mT in the samples analyzed (NSCO700 and NSCO1150). The maximum of the ZFC shifting from 212 K to 100 K and from 113 K to 40 K for the NSCO700 and NSCO1150 samples, respectively, indicates a collective freezing of the magnetic moments at lower temperature, because of the spin-glass situation. On the other hand, the shift in the irreversibility can be also associated with slower relaxation processes taking place in these samples of nanocrystals that are more weakly interacting, considering a random distribution of strong magnetic dipole-dipole interactions. Indeed, in this regard,

increasing the magnetic field implies the overcome of effects associated to the anisotropy field and dipole-dipole interactions [49,50].

Focusing the analysis on the NCSO1150 sample, its ferromagnetic and ferrimagnetic transition temperatures are in good agreement with those reported by Stauffer et al. for the $Nd_{0.75}Sr_{0.25}CoO_3$ composition [22] and with lower values than those for its lanthanum-based counterpart, as expected. In the particular case of the disordered $Ln_{0.5}Sr_{0.5}CoO_3$ compounds, the Curie temperature decreases as decreasing the cation size at the A sites [23]. According to this, for the samples annealed at lower temperatures, the values of the Curie temperature (which are higher than the expected ones for the x = 0.25 strontium doping) and the broader maxima of the dM/dT, suggest the presence of a main cobaltite phase with a slightly different level of strontium doping. Nevertheless, as the annealing temperature increases, the formed phase tends to reach the desired x = 0.25 strontium doping with its corresponding Curie temperature value, because of the correct reconfiguration of the cations in the crystalline structure stemming from the higher annealing temperature.

The evolution of the magnetization as a function of the magnetic field was studied at different temperatures (Fig. 3, right column). All samples show a hysteretic behavior and non-saturated loops. At the lowest temperature (10 K) the coercive field notably increases from a value of 304 mT for NSCO600 sample to 1279 and 1181 mT for NSCO800 and NSCO1150 samples, respectively, together with an increase of the maximum magnetization at the highest applied field, from 15.84 Am^2/kg (NSCO600 sample) to 26.47 Am^2/kg (NSC1150 sample). This also proves the reconfiguration of the cations in the crystalline structure, due to the effect of the higher annealing temperatures already mentioned. The value of the coercive field obtained for the NSCO1150 sample is higher than the one reported by Stauffer et al.[22] for the composition x = 0.25, with a value of ~900 mT versus the 1180 mT value obtained in this work. This can point to the presence of a phase separation taking place, given the fact that the coercive field is dependent on the disorder and inhomogeneities in the sample. In this regard, a clustering situation has been associated to the electronic phase separation scenario in the disordered perovskite $La_{1-x}Sr_xCoO_3$ for x > 0.3, where the coalescence of short range nanoscopic ferromagnetic clusters was reported [12,23,51]. Analogously, a long-range ferromagnetic ordering was reported to dominate over the non-ferromagnetic phases, taking the coalescence of clusters and the electronic percolation into account in the $Nd_{1-x}Sr_xCoO_3$ family (x > 0.18) [22]. Indeed, the presence of ferromagnetic clusters has been correlated to a process of doping a perovskite with a divalent cation, as favoring ferromagnetic interactions between Co^{3+} cations and the Co^{4+} obeying the Zener double-exchange mechanism [52]. These interactions coexist with the presence of antiferromagnetic interactions due to the superexchange between Co^{3+}/Co^{3+} and Co^{4+}/Co^{4+}. Furthermore, the remnant magnetization in the hysteresis loops measured at 10 K for the samples annealed at the highest temperatures (NSCO800 and NSCO1150) increases at the intermedium 50 K temperature, consistent with the existence of the ferrimagnetism stemming from the neodymium sublattice reported by neutron powder diffraction experiments at low temperature [30].

Another aspect to highlight is the fact that only the hysteresis loops of the NSCO1150 sample show a double reversal of the magnetization, better observed by the presence of two maxima (indicated by red arrows in Fig. S4d) in the derivative of the magnetization respect to the field ($dM/d(\mu_0H)$). This drop in the remnant magnetization near zero field can be attributed to the existence of two magnetic phases with different coercivities or can be explained by the presence of antiphase boundaries in the case of ordered double perovskites [24,53]. Antiphase boundaries are non-equilibrium features of crystalline solids, with a spin order different to the two magnetic regions they separate [54,55]. In this case, two ferromagnetic regions are separated by an antiphase interface where antiferromagnetic interactions occur, so that the antiparallel coupling decreases the remnant magnetization of the sample. Nevertheless, the scenario of the NSCO1150 sample seems to be more related to the oxygen deficiency, taking the disordered distribution of the Co^{3+} and Co^{4+} cations into account in the crystalline lattice. During its synthesis, the NSCO1150 sample is heated up to 1150 °C and then let cool to room temperature inside the oven. The cooling ramp under these conditions is slow enough to promote an oxygen gradient between the surface and the core in the pellets. Consequently, the coexistence of areas with different oxygen content (i.e., behaving as different phases) may explain the drop in the remnant magnetization at $\mu_0H = 0$. Though there is no evident signal for the coexistence of different ferromagnetic phases in the ZFC curve, the maximum in this curve is broad enough to hide the presence of these phases with different oxygen content within the sample. Indeed, important changes of the magnetic and transport properties of cobaltites have been directly associated to the different Co^{3+}/Co^{4+} ratio, which is related to the oxygen content of the samples [56–59].

4. Conclusions

The influence of the annealing temperature to synthesize $Nd_{0.75}Sr_{0.25}CoO_3$ nanocrystals is herein demonstrated in terms of the crystalline phases present, by means of X-ray diffraction and Raman spectroscopy, which show complementary results and point to a larger phase segregation ($Nd_xSr_yCoO_3$ and Co_3O_4) the lower the annealing temperature. In this regard, while the X-ray diffraction studies indicate the formation of a single perovskite structure for all the samples studied except for that synthesized at the lowest temperature (600 °C), Raman spectroscopy shows clearly the presence of Co_3O_4 rich regions in the samples synthesized at temperatures up to 800 °C. Furthermore, the magnetic characterization weights the crystalline phases present in the four samples, reflecting the perovskite-based magnetic behavior with ferri- and ferromagnetic transitions at ~35 K and 113 K, and the double reversal of the magnetization, attributed to an oxygen gradient within the nanocrystals synthesized at 1150 °C. Dipolar interactions and spin frustration are also reflected in these systems with a plethora of magnetic features.

CRediT authorship contribution statement

Hajer Chouaibi: Resources, Investigation, Validation, Visualization, Funding acquisition, Writing - original draft. **Beatriz Rivas-Murias:** Conceptualization, Validation, Investigation, Writing - review & editing. **Mourad Smari:** Conceptualization, Supervision. **Jalel Massoudi:** Resources, Investigation, Validation. **Essebti Dhahri:** Conceptualization, Funding acquisition. **Verónica Salgueiriño:** Conceptualization, Supervision, Writing - review & editing, Funding acquisition.

Declaration of Competing Interest

The authors declare that they have no known competing financial interests or personal relationships that could have appeared to influence the work reported in this paper.

Acknowledgment

B. R.-M. and V. S. acknowledge the financial support from the Xunta de Galicia (Regional Government, Spain) under project ED431C 2016-034 and from the Spanish Ministerio de Economía y Competitividad under project CTM2017-84050-R. Hajer Chouaibi acknowledges funding from the Tunisian Ministry of Higher Education and Scientific Research.

Appendix A. Supporting information

Supplementary data associated with this article can be found in the online version at doi:10.1016/j.jallcom.2021.159870.

References

[1] C. Ma, N. Lin, Z. Wang, S. Zhou, H. Yu, J. Lu, H. Huang, Origin of spin-state crossover and electronic reconstruction at the surface of a $LaCoO_3$ nanoparticle, Phys. Rev. B 99 (2019) 115401, https://doi.org/10.1103/PhysRevB.99.115401

[2] D.A. Gilbert, A.J. Grutter, P.D. Murray, R.V. Chopdekar, A.M. Kane, A.L. Ionin, M.S. Lee, S.R. Spurgeon, B.J. Kirby, B.B. Maranville, A.T. N'Diaye, A. Mehta, E. Arenholz, K. Liu, Y. Takamura, J.A. Borchers, Ionic tuning of cobaltites at the nanoscale, Phys. Rev. Mater. 2 (2018) 104402, https://doi.org/10.1103/PhysRevMaterials.2.104402

[3] J. Shamsi, A.S. Urban, M. Imran, L. De Trizio, L. Manna, Metal halide perovskite nanocrystals: synthesis, post-synthesis modifications, and their optical properties, Chem. Rev. 119 (2019) 3296–3348, https://doi.org/10.1021/acs.chemrev.8b00644

[4] Y. Dong, Y. Zhao, S. Zhang, Y. Dai, L. Liu, Y. Li, Q. Chen, Recent advances toward practical use of halide perovskite nanocrystals, J. Mater. Chem. A 6 (2018) 21729–21746, https://doi.org/10.1039/C8TA06376A

[5] Z. Chen, Y. Hu, J. Wang, Q. Shen, Y. Zhang, C. Ding, Y. Bai, G. Jiang, Z. Li, N. Gaponik, Boosting photocatalytic CO_2 reduction on $CsPbBr_3$ perovskite nanocrystals by immobilizing metal complexes, Chem. Mater. 32 (2020) 1517–1525, https://doi.org/10.1021/acs.chemmater.9b04582

[6] X. Zhu, Y. Lin, J. San Martin, Y. Sun, D. Zhu, Y. Yan, Lead halide perovskites for photocatalytic organic synthesis, Nat. Commun. 10 (2019) 2843, https://doi.org/10.1038/s41467-019-10634-x

[7] J. Suntivich, H.A. Gasteiger, N. Yabuuchi, H. Nakanishi, J.B. Goodenough, Y. Shao-Horn, Design principles for oxygen-reduction activity on perovskite oxide catalysts for fuel cells and metal-air batteries, Nat. Chem. 3 (2011) 546–550, https://doi.org/10.1038/nchem.1069

[8] J. Suntivich, K.J. May, H.A. Gasteiger, J.B. Goodenough, Y. Shao-horn, A perovskite oxide optimized for molecular orbital principles, Science 334 (2011) 1383–1385, https://doi.org/10.1126/science.1212858

[9] Y. Zhu, W. Zhou, J. Yu, Y. Chen, M. Liu, Z. Shao, Enhancing electrocatalytic activity of perovskite oxides by tuning cation deficiency for oxygen reduction and evolution reactions, Chem. Mater. 28 (2016) 1691–1697, https://doi.org/10.1021/acs.chemmater.5b04457

[10] J.T. Mefford, X. Rong, A.M. Abakumov, W.G. Hardin, S. Dai, A.M. Kolpak, K.P. Johnston, K.J. Stevenson, Water electrolysis on $La_{1-x}Sr_xCoO_{3-\delta}$ perovskite electrocatalysts, Nat. Commun. 7 (2016) 11053, https://doi.org/10.1038/ncomms11053

[11] J. Xu, C. Chen, Z. Han, Y. Yang, J. Li, Q. Deng, Recent advances in oxygen electrocatalysts based on perovskite oxides, Nanomaterials 9 (2019) 1161, https://doi.org/10.3390/nano9081161

[12] R. Mahendiran, A.K. Raychaudhuri, Magnetoresistance of the spin-state-transition compound $La_{1-x}Sr_xCoO_3$, Phys. Rev. B 54 (1996) 16044–16052, https://doi.org/10.1103/PhysRevB.54.16044

[13] H.M. Aarbogh, J. Wu, L. Wang, H. Zheng, J.F. Mitchell, C. Leighton, Magnetic and electronic properties of $La_{1-x}Sr_xCoO_3$ single crystals across the percolation metal-insulator transition, Phys. Rev. B 74 (2006) 134408, https://doi.org/10.1103/PhysRevB.74.134408

[14] I.O. Troyanchuk, M.V. Bushinsky, V.A. Khomchenko, V.V. Sikolenko, C. Ritter, S. Schorr, Spin state crossover and colossal magnetoresistance in barium-doped cobaltites, J. Phys. Chem. Solids 129 (2019) 86–91, https://doi.org/10.1016/j.jpcs.2018.12.035

[15] A. Maignan, T. Motohashi, S. Hébert, D. Pelloquin, B. Raveau, Cobaltites: new materials with magnetoresistance properties, Mater. Sci. Eng. B 126 (2006) 296–299, https://doi.org/10.1016/j.mseb.2005.09.029

[16] L. Zhang, X. Li, F. Wang, T. Wang, W. Shi, Colossal electroresistance and magnetoresistance effect in polycrystalline perovskite cobaltites $Nd_{1-x}Sr_xCoO_3$ (x=0.1, 0.2, 0.3), Mater. Res. Bull. 48 (2013) 1088–1092, https://doi.org/10.1016/j.materresbull.2012.11.105

[17] J.B. Goodenough, An interpretation of the magnetic properties of the perovskite-type mixed crystals $La_{1-x}Sr_xCoO_{3-\lambda}$, J. Phys. Chem. Solids 6 (1958) 287–297, https://doi.org/10.1016/0022-3697(58)90107-0

[18] M.A. Señarís-Rodríguez, J.B. Goodenough, Magnetic and transport properties of the system $La_{1-x}Sr_xCoO_{3-\delta}$ ($0 < x \leq 0.50$), J. Solid State Chem. 118 (1995) 323–336, https://doi.org/10.1006/jssc.1995.1351

[19] A. Ghoshray, B. Bandyopadhyay, K. Ghoshray, V. Morchshakov, K. Bärner, I.O. Troyanchuk, H. Nakamura, T. Kohara, G.Y. Liu, G.H. Rao, Phase separation in $Nd_{1-x}Sr_xCoO_3$ using ^{59}Co NMR, Phys. Rev. B 69 (2004) 064424, https://doi.org/10.1103/PhysRevB.69.064424

[20] J. Fan, Y. Xie, Y.-E. Yang, C. Kan, L. Ling, W. Tong, C. Wang, C. Ma, W. Sun, Y. Zhu, H. Yang, Robust electronic phase separation on nanoscale of perovskite manganite $La_{0.825}Sr_{0.175}MnO_3$, Ceram. Int. 45 (2019) 9179–9184, https://doi.org/10.1016/j.ceramint.2019.01.259

[21] S. Chattopadhyay, T.K. Nath, Electrical and magnetoelectronic properties of $La_{0.7}Sr_{0.3}MnO_3/SiO_2$/p-Si heterostructure for spintronics application, Curr. Appl. Phys. 11 (2011) 1153–1158, https://doi.org/10.1016/j.cap.2011.02.009

[22] D.D. Stauffer, C. Leighton, Magnetic phase behavior of the ferrimagnetic doped cobaltite $Nd_{1-x}Sr_xCoO_3$, Phys. Rev. B 70 (2004) 214414, https://doi.org/10.1103/PhysRevB.70.214414

[23] A.K. Kundu, Magnetic Perovskites: Synthesis, Structure and Physical Properties, Springer, 2016, https://doi.org/10.1007/978-81-322-2761-8

[24] H. Wang, J. Gazquez, C. Frontera, M.F. Chisholm, A. Pomar, B. Martinez, N. Mestres, Spontaneous cationic ordering in chemical-solution-grown La_2CoMnO_6 double perovskite thin films, NPG Asia Mater. 11 (2019) 44, https://doi.org/10.1038/s41427-019-0144-8

[25] T.L. Phan, S.K. Oh, L.V. Bau, N.X. Phuc, S.C. Yu, Spin dynamics in $La_{1-x}Sr_xCoO_3$ cobaltites, J. Magn. Magn. Mater. 300 (2006) e183–e186, https://doi.org/10.1016/j.jmmm.2005.10.221

[26] Y. Tokura, Y. Tomioka, Colossal magnetoresistive manganites, J. Magn. Magn. Mater. 200 (1999) 1–23, https://doi.org/10.1016/S0304-8853(99)00352-2

[27] J. Rodríguez-Carvajal, Recent advances in magnetic structure determination neutron powder diffraction, Phys. B 192 (1993) 55–69, https://doi.org/10.1016/0921-4526(93)90108-I

[28] P. Scherrer, Bestimmung der grösse und der inneren struktur von kolloidteilchen mittels röntgensrahlen, Nachr. Ges. Wiss. Goettingen (1918) 98–100.

[29] A.S. Panfilov, G.E. Grechnev, A.A. Lyogenkaya, V.A. Pashchenko, I.P. Zhuravleva, L.O. Vasylechko, V.M. Hreb, V.A. Turchenko, D. Novoselov, Magnetic properties of $RCoO_3$ cobaltites (R = La, Pr, Nd, Sm, Eu). Effects of hydrostatic and chemical pressure, Phys. B Condens. Matter 553 (2019) 80–87, https://doi.org/10.1016/j.physb.2018.10.036

[30] A. Krimmel, M. Reehuis, M. Paraskevopoulos, J. Hemberger, A. Loidl, Ferrimagnetic behavior of $Nd_{0.67}Sr_{0.33}CoO_3$, Phys. Rev. B 64 (2001) 224404, https://doi.org/10.1103/PhysRevB.64.224404

[31] M. Douin, L. Guerlou-Demourgues, M. Ménétrier, E. Bekaert, L. Goubault, P. Bernard, C. Delmas, Improvement by heating of the electronic conductivity of cobalt spinel phases, electrochemically synthesized in various electrolytes, J. Solid State Chem. 182 (2009) 1273–1280, https://doi.org/10.1016/j.jssc.2009.02.018

[32] M.S. Reis, D.L. Rocco, R.J.C. Vivas, B. Pimentel, N.R. Checca, R. Torrão, L. Paixão, A.M. dos Santos, Spin state and magnetic ordering of half-doped $Nd_{0.5}Sr_{0.5}CoO_3$ cobaltite, J. Magn. Magn. Mater. 422 (2017) 197–203, https://doi.org/10.1016/j.jmmm.2016.08.080

[33] E. Limpert, W.A. Stahel, M. Abbt, Log-normal distributions across the sciences: keys and clues, Bioscience 51 (2001) 341 https://doi.org/10.1641/0006-3568(2001)051[0341:LNDATS]2.0.CO;2.

[34] C. Toulouse, D. Amoroso, C. Xin, P. Veber, M.C. Hatnean, G. Balakrishnan, M. Maglione, P. Ghosez, J. Kreisel, M. Guennou, Lattice dynamics and Raman spectrum of $BaZrO_3$ single crystals, Phys. Rev. B 100 (2019) 134102, https://doi.org/10.1103/PhysRevB.100.134102

[35] L. Martín-Carrón, A. de Andrés, Melting of the cooperative Jahn-Teller distortion in $LaMnO_3$ single crystal studied by Raman spectroscopy, Eur. Phys. J. B 22 (2001) 11–16.

[36] S. Kamba, V. Goian, V. Skoromets, J. Hejtmánek, V. Bovtun, M. Kempa, F. Borodavka, P. Vanek, A.A. Belik, J.H. Lee, O. Pacherová, K.M. Rabe, Strong spin-phonon coupling in infrared and Raman spectra of $SrMnO_3$, Phys. Rev. B 89 (2014) 064308, https://doi.org/10.1103/PhysRevB.89.064308

[37] L. Martín-Carrón, A. De Andrés, Raman phonons and the Jahn-Teller transition in $RMnO_3$ manganites, J. Alloy. Compd. 323–324 (2001) 417–421, https://doi.org/10.1016/S0925-8388(01)01101-X

[38] N. Van Minh, I.S. Yang, A. Raman, scattering study of structural changes in $LaMn_{1-x}Co_xO_{3+\delta}$ system, Vib. Spectrosc. 42 (2006) 353–356, https://doi.org/10.1016/j.vibspec.2006.05.027

[39] B. Rivas-Murias, V. Salgueiriño, Thermodynamic CoO – Co_3O_4 crossover using Raman spectroscopy in magnetic octahedron- shaped nanocrystals, J. Raman Spectrosc. 48 (2017) 837–841, https://doi.org/10.1002/jrs.5129

[40] V.G. Hadjiev, M.N. Iliev, I.V. Vergilovs, The Raman spectra of Co_3O_4, J. Phys. C Solid State Phys. 21 (1988) L199–L201.

[41] O.N. Shebanova, P. Lazor, Raman study of magnetite (Fe_3O_4): laser-induced thermal effects and oxidation, J. Raman Spectrosc. 34 (2003) 845–852, https://doi.org/10.1002/jrs.1056

[42] S.D. Harvey, T.J. Peters, B.W. Wright, Safety considerations for sample analysis using a near-infrared (785 nm) Raman laser source, Appl. Spectrosc. 57 (2003) 580–587, https://doi.org/10.1366/000370203321666632

[43] D.N.H. Nam, K. Jonason, P. Nordblad, N.V. Khiem, N.X. Phuc, Coexistence of ferromagnetic and glassy behavior in the $La_{0.5}Sr_{0.5}CoO_3$ perovskite compound, Phys. Rev. B 59 (1999) 4189–4194, https://doi.org/10.1103/PhysRevB.59.4189

[44] D.N.H. Nam, R. Mathieu, P. Nordblad, N.V. Khiem, N.X. Phuc, Spin-glass dynamics of $La_{0.95}Sr_{0.05}CoO_3$, Phys. Rev. B 62 (2000) 8989–8995, https://doi.org/10.1103/PhysRevB.62.8989

[45] M. Itoh, I. Natori, S. Kubota, K. Motoya, Hole-doping effect on magnetic properties of $La_{1-x}Sr_xCoO_3$ ($0 \leq x \leq 0.5$), J. Magn. Magn. Mater. 140–144 (1995) 1811–1812, https://doi.org/10.1016/0304-8853(94)00677-6

[46] N.X. Phuc, N. [Van Khiem], D.N.H. Nam, Field dependence of zero-field-cooled magnetization of $La_{1-x}Sr_xCoO_3$ (x=0.05–0.5), J. Magn. Magn. Mater. 242–245 (2002) 754–756, https://doi.org/10.1016/S0304-8853(01)01020-4

[47] J. Wu, C. Leighton, Glassy ferromagnetism and magnetic phase separation in $La_{1-x}Sr_xCoO_3$, Phys. Rev. B 67 (2003) 174408, https://doi.org/10.1103/PhysRevB.67.174408

[48] V. Salgueiriño-Maceira, M.A. Correa-Duarte, M. Bañobre-López, M. Grzelczak, M. Farle, L.M. Liz-Marzán, J. Rivas, Magnetic properties of Ni/NiO nanowires deposited onto CNT/Pt nanocomposites, Adv. Funct. Mater. 18 (2008) 616–621, https://doi.org/10.1002/adfm.200700846

[49] C. Antoniak, J. Lindner, V. Salgueiriño-Maceira, M. Farle, Multifrequency magnetic resonance and blocking behavior of Fe_xPt_{1-x} nanoparticles, Phys. Status Solidi A 203 (2006) 2968–2973, https://doi.org/10.1002/pssa.200567114

[50] P. Zhang, F. Zuo, F.K. Urban, A. Khabari, P. Griffiths, A. Hosseini-Tehrani, Irreversible magnetization in nickel nanoparticles, J. Magn. Magn. Mater. 225 (2001) 337–345, https://doi.org/10.1016/S0304-8853(00)01379-2
[51] P.L. Kuhns, M.J.R. Hoch, W.G. Moulton, A.P. Reyes, J. Wu, C. Leighton, Magnetic phase separation in $La_{1-x}Sr_xCoO_3$ by ^{59}Co nuclear magnetic resonance, Phys. Rev. Lett. 91 (2003) 95–98, https://doi.org/10.1103/PhysRevLett.91.127202
[52] J.B. Goodenough, Magnetism and the Chemical Bond, Interscience Publishers, New York, 1963.
[53] R.I. Dass, J.B. Goodenough, Multiple magnetic phases of $La_2CoMnO_{6-\delta}$ ($0 \le \delta \le 0.05$), Phys. Rev. B 67 (2003) 144011–144019, https://doi.org/10.1103/physrevb.67.014401
[54] Y. Murakami, K. Niitsu, T. Tanigaki, R. Kainuma, H.S. Park, D. Shindo, Magnetization amplified by structural disorder within nanometre-scale interface region, Nat. Commun. 5 (2014) 4133, https://doi.org/10.1038/ncomms5133
[55] N. Fontaiña-Troitiño, M.A. Ramos-Docampo, M. Testa-Anta, B. Rodríguez-González, M. Bañobre-López, L. Bocher, K.P. McKenna, V. Salgueiriño, Antiphase boundaries in truncated octahedron-shaped Zn-doped magnetite nanocrystals, J. Mater. Chem. C 6 (2018) 12800–12807, https://doi.org/10.1039/C8TC05731A
[56] S. Streule, A. Podlesnyak, J. Mesot, M. Medarde, K. Conder, E. Pomjakushina, E. Mitberg, V. Kozhevnikov, Effect of oxygen ordering on the structural and magnetic properties of the layered perovskites, J. Phys. Condens. Matter 17 (2005) 3317–3324, https://doi.org/10.1088/0953-8984/17/21/024
[57] C. Frontera, J.L. García-Muñoz, A.E. Carrillo, A. Caneiro, C. Ritter, D. Martín y Marero, Magnetism and vacancy ordering in $PrBaCo_2O_{5+\delta}$ ($\delta \geqslant 0.50$), J. Appl. Phys. 97 (2005) 10C106, https://doi.org/10.1063/1.1855017
[58] B. Rivas-Murias, M. Sánchez-Andújar, J. Rivas, M.A. Señarís-Rodríguez, Influence of the oxygen content and the preparation method on the power factor of $PrBaCo_2O_{5+\delta}$ samples ($0.54 \le \delta \le 0.84$), J. Alloy. Compd. 509 (2011) 5250–5255, https://doi.org/10.1016/j.jallcom.2011.01.217
[59] S. Ganorkar, K.R. Priolkar, P.R. Sarode, A. Banerjee, Effect of oxygen content on magnetic properties of layered cobaltites $PrBaCo_2O_{5+\delta}$, J. Appl. Phys. 110 (2011) 053923, https://doi.org/10.1063/1.3633521